Mechanistic Study of Silica Nanoparticles on the Size-dependent Retinal Toxicity *in Vitro* and *in Vivo*

Zhuhong Zhang (zhzhang0608@ytu.edu.cn)
Yantai University https://orcid.org/0000-0001-6720-0996
Laien Zhao
Yantai University
Yuanyuan Ma
Yantai University
Jia Liu
Yantai University
Yanmei Huang
Yantai University
Xiaoxuan Fu
Yantai University
Shengjun Peng
Yantai University
Xiaojie Wang
Yantai University
Yun Yang
Yantai University
Xiaoyan Zhang
Yantai University
Wanru Ding
Yantai University
Jinguo Yu
Tianjin Medical University General Hospital
Yanping Zhu
Yantai University
Hua Yan
Tianjin Medical University General Hospital
Shubin Yang
Yantai University

Research

Keywords: SiO2 NPs, retinal toxicity, ROS, ganglion cell degeneration, glial cell activation, inflammation

Posted Date: January 3rd, 2022

DOI: https://doi.org/10.21203/rs.3.rs-1201444/v1

Version of Record: A version of this preprint was published at Journal of Nanobiotechnology on March 19th, 2022. See the published version at https://doi.org/10.1186/s12951-022-01326-8.

Abstract

Background: Silica nanoparticles (SiO_2 NPs) are extensively applied in the biomedical field. The increasing medical application of SiO_2 NPs has raised concerns about their safety. However, studies on SiO_2 NP-induced retinal toxicity are lacking.

Methods: We investigated the retinal toxicity of SiO_2 NPs with different sizes (15 and 50 nm) *in vitro* and *in vivo* along with the underlying mechanisms. The cytotoxicity of SiO_2 NPs with different sizes was assessed in R28 human retinal precursor cells by determining the ATP content and LDH release. The cell morphologies and nanoparticle distributions in the cells were analyzed by phase-contrast microscopy and transmission electron microscopy, respectively. The mitochondrial membrane potential was examined by confocal laser scanning microscopy. The retinal toxicity induced by SiO_2 NPs *in vivo* was examined by immunohistochemical analysis. To further investigate the mechanism of retinal toxicity induced by SiO_2 NPs, reactive oxygen species (ROS) generation, glial cell activation and inflammation were monitored.

Results: The 15-nm SiO_2 NPs were found to have higher cytotoxicity than the larger NPs. Notably, the 15-nm SiO_2 NPs induced retinal toxicity *in vivo*, as demonstrated by increased cell death in the retina, TUNEL-stained retinal cells, retinal ganglion cell degeneration, glial cell activation, and inflammation. In addition, The SiO_2 NPs caused oxidative stress, as demonstrated by the increase in the ROS indicator H_2DCF-DA. Furthermore, the pretreatment of R28 cells with N-acetylcysteine, an ROS scavenger, attenuated the ROS production and cytotoxicity induced by SiO_2 NPs.

Conclusions: These results provide evidence that SiO_2 NPs induce size-dependent retinal toxicity and suggest that glial cell activation and ROS generation contribute to this toxicity.

1. Introduction

Due to the wide application of nanomaterials in various fields, they are being increasingly manufactured. Silica nanoparticles (SiO_2 NPs) are abundant in the Earth, and over 100 SiO_2 NP products have been released on the global market [1–3]. In the last decade, SiO_2 NPs have shown promise for applications in the biomedical field, including in disease labeling, biosensors, and the delivery of drugs and vaccines, due to their thermal stability and biocompatibility [4, 5]. Mesoporous and core/shell SiO_2 NPs have been developed for tumor imaging and therapy [6]. In addition, SiO_2 NPs have been reported for application in the treatment of ocular diseases. For example, SiO_2 NPs loaded with a nitric oxide donor can be used to treat primary open-angle glaucoma [7]. The intravitreal injection of SiO_2 NPs was shown to significantly inhibit retinal angiogenesis in oxygen-induced retinopathy mice [8]. However, the growing potential for human exposure to SiO_2 NPs has attracted concern surrounding human health.

Some *in vivo* and *in vitro* studies have shown that SiO_2 NPs can cause toxicity to different organs in the human body; toxicity has been demonstrated in lung epithelial cells [9], liver cells [10], intestinal cells [11], the lungs [12], and kidneys [13]. In addition, SiO_2 NPs were found to induce genotoxicity and alterations in gene and protein expression [12, 14], and Chen et al. [15] reported that SiO_2 NPs can induce cornea toxicity. The local ocular delivery of medicine has become an important strategy for treating retinal diseases [16–18], and intravitreal injection has become a common treatment method for various retinal diseases including diabetic retinopathy, macular degeneration, macular edema, and inflammatory diseases [19, 20]. However, the use of intravitreal drugs can result in retinal toxicity [21]. For example, silver nanoparticles were found to induce apoptosis in the human retinal pigment epithelia cell line ARPE-19 *in vitro* [22]. Wang et al. [23] reported that ZnO nanoparticles induced murine photoreceptor cell death *in vitro*. Nanomaterials can also induce ocular inflammation [24], and inflammation of the retinal tissue can lead to the secretion of cytokines and retinal damage. However, little is currently known about the retinal toxicity induced by SiO_2 NPs *in vitro* and *in vivo*.

The effects of nanomaterials on cells may be influenced by various properties, including the nanomaterial's crystallinity, size, shape, and surface area. Natural silica can exist in two states: crystalline and amorphous. Crystalline silica can easily lead to silicosis and lung cancer and is classified as a Group 1 carcinogen by the International Agency for Research on Cancer (IARC) [1] [25]. Notably, the toxicity of amorphous SiO_2 NPs has begun to attract the attention of scientists in recent years. Mice treated with 70-, 300-, and 1000-nm amorphous SiO_2 NPs showed no changes in hematology, histopathology, or biochemistry [26]; in contrast, Liu et al. [1] found that amorphous SiO_2 NPs induced inflammation in HUVEC cells by activating the HMGB1/TLR4/MYD88/NF-kb signaling pathway. Tassinari et al. [27] that amorphous SiO_2 NPs induced acute toxicity in the liver and spleen of male and female rats after intravenous administration. Brandão et al. [12] demonstrated that amorphous SiO_2 NPs induced genotoxicity in lung cells. Particle size is also an important factor affecting the toxicity of SiO_2 NPs. For example, in the A549 cell line, SiO_2 NPs induced higher toxicity than SiO_2 microparticles [28]. An *in vitro* study showed that SiO_2 NP-induced toxicity depends not only on the particle size, but also on the cell type [29]. In the present study, we investigated the effect of amorphous SiO_2 NP size on retinal toxicity.

The mechanism of SiO_2 NP-induced toxicity remains unclear. One potential mechanism by which SiO_2 NPs might induce retinal toxicity involves reactive oxygen species (ROS). Some reports have suggested that SiO_2 NPs can induce ROS production in various cell lines, including human keratinocytes [30], human HK-2 cells [31], and HUVEC cells [1]. Many studies have indicated that ROS are closely related to cytotoxicity [32, 33], and the inhibition of ROS can ameliorate the cytotoxicity. Other studies have demonstrated that SiO_2 NPs can induce inflammation [11], and oxidative stress and inflammation are thought to be closely related to the toxicity induced by nanoparticles.

Previous studies generally focused on a limited number of endpoints; in contrast, in the current study, we implemented a comprehensive set of tests to assess the potential effects of SiO_2 NPs on the retina and

retinal cells. More specifically, the cytotoxicity, morphological changes, and localization of SiO_2 NPs in R28 cells induced by SiO_2 NPs with two different sizes (15 and 50 nm) were investigated. We also determined the role of SiO_2 NPs in in the apoptosis of retinal cells and the damage of retinal ganglion cells (RGCs). In addition, we explored the potential role of glial cell activation, inflammation and ROS accumulation in SiO_2 NP-induced retinal toxicity (Scheme 1).

2. Experimental Section

2.1 Chemicals and reagents

SiO_2 NPs were purchased from Shanghai Macklin Biochemical Co., Ltd (Shanghai, China). Fetal bovine serum (FBS), Dulbecco's modified eagle medium (DMEM), and penicillin/streptomycin were obtained from Life Technologies (Carlsbad, CA, USA). N-acetylcysteine (NAC) and 2',7'-dichlorofluorescin diacetate (H_2DCF-DA) were purchased from Sigma-Aldrich (St. Louis, MO, USA). A JC-1 mitochondrial membrane potential assay kit was purchased from Beyotime Biotechnology Co., Ltd. (Shanghai, China).

2.2 Characterization of SiO_2 NPs

The sizes and morphologies of the SiO_2 NPs were evaluated by transmission electron microscopy (TEM; Tecnai F20, Philips, Netherlands, 200kV) and field-emission scanning electron microscopy (FE-SEM; JEOL JSM-7001F). The crystal structures of the SiO_2 NPs were examined by powder X-ray diffraction (XRD) using monochromic Cu-Kα radiation (Rigaku Smart Lab, Japanese Neo Confucianism, Japan) at 40 kV and 300 mA.

2.3 Cell culture

The retinal precursor cell line R28 was obtained from Kerafast (Boston, MA, USA) and cultured according to the supplier's instructions. The cells were cultured in DMEM+, which contained 420 mL DMEM (Sigma-Aldrich, St. Louis, MO, USA), 15 mL sodium bicarbonate (Sigma-Aldrich, St. Louis, MO, USA), 50 mL calf serum (Hylone), 5 mL MEM non-essential amino acids (GIBCO), 5 mL L-glutamine (GIBCO), and 0.625 mL Gentamicin (80 mg/mL; Solarbio Life Sciences Co., Ltd, Beijing, China). The cells were maintained at 37°C in a humidified atmosphere containing 5% CO_2. Next, the SiO_2 NPs were dispersed in ultrapure water to prepare a stock solution (200 mg/mL). The stock solution was sonicated using a probe sonicator (Ningbo Xinzhi Biotechnology Co., Ltd., Ningbo, China) at 600 W for 40 min and diluted to different concentrations with culture medium just before cell exposure. The cells were adjusted to a concentration of 1×10^5 cells/mL in a volume of 100 μL per well in 96-well plates for toxicity assays.

2.4 Cell morphology

R28 cells were seeded in 96-well plates at a density of 1×10^4 cells/well and cultured overnight in a CO_2 incubator. The cells were exposed to SiO_2 NPs at different concentrations (5–80 μg/mL) for 12 and 24 h.

The changes in cell morphology were examined using a phase-contrast microscope (Leica DM16000B, Heidelberg, Germany).

2.5 Uptake of SiO_2 NPs

To examine the localization of SiO_2 NPs in R28 cells, R28 cells were plated in six-well plates, cultured overnight, and treated with SiO_2 NPs (20 μg/mL) for 24-h. The R28 cells were then collected, washed three times with phosphate-buffered saline (PBS), and fixed with 2.5% glutaraldehyde solution at 4°C overnight. After the fixed cells were dehydrated, serial ultrathin sections were created and examined by TEM (Hitachi H7650, Japan).

2.6 Detection of mitochondrial membrane potential

The SiO_2 NP-induced changes in mitochondrial membrane potential were assessed as previously described [34]. Briefly, R28 cells were seeded in dishes at a density of 1×10^5 cells/mL and cultured overnight. The cells we treated with different concentrations of SiO_2 NPs for 6, 12 and 24 h. Following treatment, the cells were washed three times with PBS and then incubated with JC-1 (20 μM; Beyotime, Beijing, China) for 15 min. After removing the JC-1 staining solution, the cells were washed three times, and PBS was added for imaging by confocal laser scanning microscopy (CLSM; ZEISS LSM 800, Germany).

2.7 Intravitreal injection of SiO_2

Three-week-old male Sprague–Dawley rats were purchased from Pengyue Experimental Animal Company (Jinan, China). All animal procedures were carried out in accordance with the National Institutes of Health Guide for the Care and Use of Laboratory Animals and were in compliance with the ARVO Statement for the Use of Animals in Ophthalmic and Vision Research. Animal protocols were approved by the Committee of Yantai University for the Care and Use of Laboratory Animals. All rats were housed under 12-h dark/light cycles at 23°C ± 1°C, and food and water were available *ad libitum*. Prior to intravitreal injection, the rats were anesthetized via the intraperitoneal injection of ketamine (100 mg/kg) and xylazine (7 mg/kg), and the pupils were anesthetized with 0.5% proxymetacaine hydrochloride. The rats were randomly divided into three groups: sham, vehicle control (PBS), and SiO_2 NPs. Intravitreal injections were carried out using a 30-gauge needle attached to a 1-mL syringe; 5 μL of SiO_2 NP suspension was injected to obtain a final concentration of 80 μg/mL in the vitreous humor.

2.8 TUNEL assay

Assays were performed using a one-step TUNEL Apoptosis Assay Kit (Beyotime) following the manufacturer's instructions. Briefly, cryosections were stained using the kit to test DNA fragmentation as an indicator of cell death. To count TUNEL-positive cells, three sections from each rat were imaged by confocal laser scanning microscopy (CLSM; ZEISS LSM 800, Germany). The counts from all sections of the same animal were averaged, and the data from six rats were used to obtain the average and standard deviation (SD) for the group.

2.9 Evaluation of retinal ganglion cells (RGCs) and inflammatory markers in SiO2 NP-injected retinas

Cryosections were stained with primary antibodies in blocking solution overnight at 4°C prior to incubation with secondary antibodies diluted in blocking solution for 1 h at room temperature. Nuclei were stained with 4',6-diamidino-2-phenylindole (DAPI). The primary antibodies were as follows: mouse anti-β-III-tubulin (1:100, Beyotime), rabbit anti-glial fibrillary acid protein (anti-GFAP; 1:100, Beyotime), rabbit anti-TNF-α (1:100, Beyotime), and IL-1β (1:100, Beyotime). To quantify immunofluorescence intensity, the areas of β-III-tubulin and GFAP immunopositivity were determined by thresholding based on the images obtained using Image J (National Institutes of Health, Bethesda, MD, USA). TNF-α- and IL-1β-positive cells were quantified from at least three sections of each rat. Each group included six rats. Comparisons between groups were made using one-way analysis of variance (ANOVA).

2.10 Measurement of ROS

Intracellular ROS production was assessed using H_2DCF-DA staining as previously described [34]. Briefly, R28 cells were treated with 10 μM H_2DCF-DA for 30 min in the cell culture incubator. The cells were washed with PBS to remove unincorporated dye and then treated with 5–80 μg/mL SiO_2 NPs in phenol red-free medium. The cells were incubated for 24 h, and the fluorescence intensity was measured after 2, 4, 6, 12, and 24 h using a Synergy H4 Hybrid microplate reader. Meanwhile, the oxidation of H_2DCF-DA was detected by CLSM (ZEISS LSM 800, Germany) at the same time points.

2.11 Statistical analysis

All data are presented as the mean ± SD. Statistical analysis was performed using Graph Pad Prism 6 (La Jolla, CA, USA). Treatment-related differences were evaluated by one-way ANOVA followed by Dunnett's tests (for comparisons of different concentrations to the vehicle control) or by two-way ANOVA followed by Tukey's multiple comparison test (for comparisons of two treatment groups in NAC pretreatment experiments). A difference was considered statistically significant when the *p* value was less than 0.05.

3. Results

3.1 Characterization of SiO_2 NPs

The wide application of SiO_2 NPs in the biomedical field has raised concerns regarding the safety of these NPs in humans and the environment. While the cytotoxicity of SiO_2 NPs has been investigated by numerous scientists [3, 5, 35], most of these studies explored various SiO_2 NP characteristics using a wide variety of *in vitro* models. Until now, no study has evaluated the retinal toxicity either *in vitro* or *in vivo*. In the present study, we explored the retinal toxicity of two types of SiO_2 NPs with different sizes both *in vitro* and *in vivo*. We also investigated the potential mechanism underlying the retinal toxicity induced by SiO_2 NPs.

Recently, SiO_2 NPs have shown great potential in the treatment of ocular diseases [36–39]. Given the widespread use of SiO_2 NPs to treat ocular diseases, the ocular toxicity of SiO_2 NPs requires more attention from scientists and ophthalmologists. Park et al. reported that SiO_2 NPs with sizes of 50, 100, and 150 nm did not induce significant cytotoxicity in cultured human corneal epithelial cells [40]. However, Chen et al. reported that SiO_2 NPs led to cytotoxicity, ROS generation, and DNA damage in the human cornea [15]. SiO_2 NPs can be used as intravitreal drug carriers [38, 41]; however, to the best of our knowledge, the retinal toxicity of SiO_2 NPs has not been investigated before now. Therefore, we conducted both *in vitro* and *in vivo* experiments to evaluate the retinal toxicity of SiO_2 NPs with sizes of 15 and 50 nm. The *in vitro* study used human R28 retinal precursor cells, which are expected to mimic *in vivo* responses.

We first evaluated the effect of SiO_2 NP size on retinal toxicity. The morphology, size, and structure the of SiO_2 NPs were characterized by SEM, TEM, and XRD, respectively. The SEM images of the two types of SiO_2 NPs (Figs. 1A **& B**) indicate that both NPs had spherical morphologies. The TEM images (insets of Figs. 1A **& B**) show that the SiO_2 NPs had sizes of approximately 15 and 50 nm and were slightly aggregated in aqueous solution. Based on the XRD spectra (Figs. 1C **& D**), both types of SiO_2 NPs were amorphous.

3.2 Cytotoxicity of SiO2 NPs in R28 cells

We compared the cytotoxicity of the SiO_2 NPs with different sizes (15 and 50 nm) in human R28 retinal precursor cells. Cytotoxicity was determined by adenosine triphosphate (ATP) assay and lactate dehydrogenase (LDH) release assay. (Fig. 2). The R28 cells were treated with the two types of SiO_2 NPs at various concentrations ranging from 5–80 μg/mL for 12 and 24 h. As shown in Fig. 2, the SiO_2 NPs induced significant time- and concentration-dependent decreases in ATP content (Figs. 2A **& B**) and LDH release (Fig. 2C **& D**). Among the two types of SiO_2 NPs, the R28 cells showed greater sensitivity to the 15-nm SiO_2 NPs.

3.3 SiO_2 NPs induce morphological changes in R28 cells

The morphology of the R28 cells changed as the SiO_2 NP concentration increased. After 12 h, the cell morphology became irregular when the NP concentration reached 20 (50-nm SiO_2 NPs; Fig. 3A) or 40 μg/mL (50-nm SiO_2 NPs; Fig. 3A). At 24 h, the changes in cell morphology became more prominent with increasing SiO_2 NP concentration (Fig. 3B) At the concentration of 80 μg/mL, most cells were detached, and the density was obviously reduced.

3.4 In vitro localization of SiO_2 NPs in R28 cells

The *in vitro* distributions of SiO_2 NPs with sizes of 15 and 50 nm in R28 cells were evaluated by TEM. In R28 cells before SiO_2 NP treatment, no SiO_2 NPs were observed in the nucleus or cytosol (Fig. 4). After

exposure for 24 h, both 15- and 50-nm SiO_2 NPs were visible in the cytoplasm, and some 15-nm SiO_2 NPs were found in the mitochondria.

3.5 SiO_2 NPs induce mitochondrial dysfunction

As the 15-nm SiO_2 NPs accumulated in the mitochondria, we measured the change in mitochondrial depolarization (ΔΨm) in R28 cells treated with 15-nm SiO_2 NPs. The value of ΔΨm was measured using JC-1 dye. The R28 cells were treated with SiO_2 NPs at concentrations of 20, 40, and 80 μg/mL for 6, 12, and 24 h. Decreases in mitochondrial depolarization in the R28 cells were observed as early as 6 h after treatment with 80 μg/mL SiO_2 NPs (Fig. 5A). As shown by the JC-1 staining images (Fig. 5C), the transition from red fluorescence to green fluorescence became more obvious at 24 h after treatment, suggesting that the SiO_2 NPs induced a significant time- and concentration-dependent decrease in mitochondrial depolarization (Fig. 5). Consequently, in subsequent experiments, the SiO_2 NP concentration of 80 μg/mL was used to investigate the retinal toxicity *in vivo*.

3.6 SiO_2 NPs induce retinal toxicity in vivo

To examine the retinal toxicity of SiO_2 NPs *in vivo*, SiO_2 NPs were intravitreally injected. At 1, 7, and 14 d after injection, the rats were euthanized, and frozen sections of the retina were prepared for fluorescence staining. The retina shape became irregular at 7 d after injection, and the retinas became very loose at 14 d after injection. Notably, many cells infiltrated into the retinal ganglion cell layer (GCL); these cells were suspected to be inflammatory cells. To measure retinal cell death after SiO_2 NP injection, cells stained with DAPI were counted in the outer nuclear layer (ONL), inner nuclear layer (INL), and GCL. The number of cells decreased with time after injection in the ONL, INL, and GCL, and the overall number of cells also decreased (Fig. 6). Next, retinal cryosections were analyzed by TUNEL apoptosis assay (Fig. 7). The percentage of apoptotic cells increased in the SiO_2 NP-treated groups in a time-dependent manner. Compared to the sham group, the intravitreal injection of SiO_2 NPs increased the number of TUNEL-positive cells by approximately 4-, 16-, and 32-fold after 1, 7, and 14 d, respectively.

3.7 SiO_2 NPs activate the inflammatory response in vivo

As mentioned above, cells that we suspected to be inflammatory cells infiltrated the GCL. Thus, we investigated whether the SiO_2 NPs caused retinal inflammation. GFAP, a marker of glial cells in the retina, was assessed by immunofluorescence staining. As demonstrated in Fig. 8, glial cells were obviously activated as early as 1 d after the injection of SiO_2 NPs, and the number of activated glial cells rose sharply at 7 d after injection (Figs. 8A **& B**). The maximum GFAP signal induction was approximately 60 times that of the PBS control at 14 d after injection (Fig. 8C). RGCs can be damaged by various stimuli such as inflammation, ischemia, oxidative stress, and excitotoxicity [42]. Therefore, to understand whether the activation of glial cells can damage RGCs, we evaluated the expression of β-III-tubulin, a marker of RGCs. As shown in Fig. 8A, at 1 d after SiO_2 NP injection, the RGCs (β-III-tubulin positive) were reduced by 52% compared to the vehicle control. The cell number decreased more predominately at 7 and

14 d after injection (Figs. 8B **& C**). These findings demonstrate that the intravitreal injection of SiO_2 NPs activated glial cells and damaged RGCs.

As SiO_2 NPshave been demonstrated to induce inflammation in HUVEC cells [1], and pro-inflammatory cytokines (e.g., TNF-α and IL-1β) secreted by macrophages play a crucial role in the inflammation process, we investigated whether the SiO_2 NPs induced the secretion of TNF-α and IL-1β. The retinas were stained with antibodies against TNF-α and IL-1β and assessed by immunofluorescence staining. The levels of TNF-αand IL-1β were notably increased in the group injected with SiO_2 NPs compared to the control. For example, the number ofIL-1β-positive cells increased by 8- and 23-fold compared to the vehicle control at 1 and 7 d after SiO_2 NP injection, respectively (**Figs.9A & B**); the number of TNF-α-positive cells showed similar trends (**Figs.9C & D**).

Taken together, the above results indicate that the SiO_2 NPs caused retinal cell death and activated retinal inflammation.

3.8 SiO_2 NPs cause ROS overproduction

Driven by the *in vitro* and *in vivo* effects of SiO_2 NPs on cell viability, morphology, mitochondrial dysfunction, apoptosis, and inflammation, we investigated the potential mechanisms underlying the retinal toxicity of SiO_2 NPs. Previous studies demonstrated that one of the main toxicity mechanisms of NPs involves ROS generation [15, 23, 43]. Therefore, we first investigated whether the 15-and 50-nm SiO_2 NPs induced oxidative stress. R28 cells were treated with SiO_2 NPs at concentrations ranging from 5 to 80 μg/mL, and ROS production was monitored at 2, 4, 6, 12, and 24 h after treatment (Fig. 10). The SiO_2 NPs were found to have size-, time-, and concentration-dependent effects on ROS generation. Compared with the control group, the ROS levels increased significantly within 2 h of treatment with 15-nm SiO_2 NPs at 80 μg/ml. The ROS level continued to increase dramatically over time, reaching a maximum value (approximately 3 times that of the control group) at 6 h after treatment with 15-nm SiO_2 NPs (Fig. 10A). Similarly, the ROS level increased significantly at 4 h after treatment with 50-nm SiO_2 NPs (80 μg/mL); the maximum ROS level (2.3 times that of the control) occurred at 6 h after treatment (Fig. 10C). The ROS levels then decreased from 6 h to 12 and 24 h after treatment, presumably due to reduced cell growth (Fig. 2). To further verify the ROS generation results, we performed ROS uorescence staining. R28 cells were treated with 15- and 50-nm SiO_2 NPs at concentrations of 20 and 80 μg/mL. The CLSM images show that the ROS levels increased with incubation time (Figs. 10B **& D**). The increase in ROS level suggests that treatment with SiO_2 NPs resulted in oxidative stress. Subsequent assays focused on the 15-nm SiO_2 NPs.

3.9 SiO_2 NP-induced retinal toxicity is attenuated by ROS scavenging

To further investigate the role of ROS generation in the retinal toxicity of SiO_2 NPs, we used NAC, a ROS scavenger, to inhibit intracellular ROS generation. R28 cells were pretreated with NAC (10 mmol) for 1 h prior to treatment with SiO_2 NPs (5–80 μg/ml) for 12 h. As shown in Fig. 11A, NAC significantly attenuated ROS induction. To further verify this result, we performed ROS uorescence staining. The CLSM images show that pretreating cells with NAC before treatment with 40 μg/mL SiO_2 NPs inhibited ROS production (Fig. 11B). Finally, the pretreatment of cells with NAC significantly decreased SiO_2 NP-induced retinal toxicity in the R28 cells, as evidenced by the reduction in ATP content (Fig. 11C). These findings indicate that SiO_2 NP-induced retinal toxicity was partially mediated by ROS generation.

4. Discussion

The wide application of SiO_2 NPs in the biomedical field has raised concerns regarding the safety of these NPs in humans and the environment. While the cytotoxicity of SiO_2 NPs has been investigated by numerous scientists [3, 5, 35], most of these studies explored various SiO_2 NP characteristics using a wide variety of *in vitro* models. Until now, no study has evaluated the retinal toxicity either *in vitro* or *in vivo*. In the present study, we explored the retinal toxicity of two types of SiO_2 NPs with different sizes both *in vitro* and *in vivo*. We also investigated the potential mechanism underlying the retinal toxicity induced by SiO_2 NPs.

Recently, SiO_2 NPs have shown great potential in the treatment of ocular diseases [36–39]. Given the widespread use of SiO_2 NPs to treat ocular diseases, the ocular toxicity of SiO_2 NPs requires more attention from scientists and ophthalmologists. Park et al. reported that SiO_2 NPs with sizes of 50, 100, and 150 nm did not induce significant cytotoxicity in cultured human corneal epithelial cells [40]. However, Chen et al. reported that SiO_2 NPs led to cytotoxicity, ROS generation, and DNA damage in the human cornea [15]. SiO_2 NPs can be used as intravitreal drug carriers [38, 41]; however, to the best of our knowledge, the retinal toxicity of SiO_2 NPs has not been investigated before now. Therefore, we conducted both *in vitro* and *in vivo* experiments to evaluate the retinal toxicity of SiO_2 NPs with sizes of 15 and 50 nm. The *in vitro* study used human R28 retinal precursor cells, which are expected to mimic *in vivo* responses.

We first evaluated the effect of SiO_2 NP size on retinal toxicity. First, the particle morphology and average size were examined by SEM and TEM (Fig. 1). The two types of SiO_2 NPs had sizes of 15 ± 5 and 50 ± 5 nm. The 15-nm particles showed greater toxicity in R28 cells than the 50-nm particles (Figs. 2 and 3), consistent with previous studies on the effect of NP size on toxicity [1, 11, 44]. TEM imaging showed that both sizes of SiO_2 NPs were uptaken by R28 cells within 24 h and localized within the cytoplasm (Fig. 4). Importantly, the 15-nm SiO_2 NPs were found in the mitochondria in addition to in the cytoplasm, which may explain why the 15-nm SiO_2 NPs were more toxic than the 50-nm particles. Chen et al. [45] observed 70-nm SiO_2 NPs in the nuclei of human epithelial HEp-2 cell; however, the nuclear translocation of SiO_2 NPs was not observed in the current study. The localization of NPs in cells can cause changes in cell morphology [46]. Thus, we evaluated the effects of the 15- and 50-nm SiO_2 NPs on R28 cell morphology.

Treatment with SiO_2 NPs led to size-, time-, and concentration-dependent decreases in cell density and caused the cell shape to become ambiguous (Fig. 3).

As mentioned above, the 15-nm SiO_2 NPs were more toxic than the 50-nm particles, consistent with previous studies finding that smaller particles tend to have higher cytotoxicity than larger particles. Thus, subsequent toxicity assays focused on the 15-nm SiO_2 NPs. Mitochondria play a key role in cell survival and are the primary location of ATP production. Mitochondrial depolarization can lead to a decrease in ATP level. In this study, the SiO_2 NPs induced mitochondrial dysfunction (Fig. 5).

Because the concentration of SiO_2 NPs used as a drug carrier was reported to be 100 μg/mL [38], we studied the *in vivo* retinal toxicity of SiO_2 NPs at a concentration of 80 μg/mL, which was the highest concentration used in our *in vitro* experiments. First, cell death and TUNEL assays were performed. Consistent with the *in vitro* results, the SiO_2 NPs showed time-dependent toxicity in the retina (Figs. 6 and 7). Meanwhile, cells suspected to be inflammatory cells were observed in the GCL. Inflammation is the key factor in RGC damage. Importantly, the injection of SiO_2 NPs induced glial cell activation and RGC damage in a time-dependent manner (Fig. 8). Our data also indicate that the injection of SiO_2 NPs induced the pro-inflammatory cytokines TNF-α and IL-1β. Therefore, inflammation may be a factor in the retinal toxicity induced by SiO_2 NPs.

Oxidative stress is the most studied factor in NP-induced toxicity because the small sizes and large surface areas of NPs are thought to generate ROS and induce oxidative stress [47]. After the cell is adversely stimulated, the mitochondria produce excess ROS due to an imbalance between ROS formation and the activity of the cellular antioxidant system. If the ROS cannot be completely degraded, the excess ROS will cause oxidative stress and induce cytotoxicity, leading to cell death [48]. Recent studies found that amorphous SiO_2 led to ROS generation in MRC-5 human lung fibroblast cells [43] and MH-S macrophage cells [49]. Interestingly, the present study demonstrated that 15- and 50-nm SiO_2 NPs also caused ROS generation in R28 cells in a size- and dose-dependent manner for the first time (**Fig. 9**). Furthermore, the SiO_2 NP-induced cytotoxicity in R28 cells was attenuated by pretreating the cells with NAC, an antioxidant (Fig. 10). This finding is in good agreement with a previous study in which cellular damage in vascular endothelial cells was attributed to the pro-oxidant effect of SiO_2 NPs [4].

Conclusion

In summary, in the current study, both 15- and 50-nm SiO_2 NPs induced cytotoxicity in R28 cells *in vitro*. Based on the decrease in ATP, LDH release, localization in the mitochondria, and ROS generation, the 15-nm SiO_2 NPs were more toxic than the 50-nm NPs. The 15-nm SiO_2 NPs also induced retinal toxicity and activated inflammatory response *in vivo*. ROS overproduction seems to play a critical role in the retinal toxicity induced by SiO_2 NPs. The results provide new insights into the mechanism of SiO_2 NP-induced retinal toxicity and improve our understanding of the potential hazards associated with the use of SiO_2 NPs. It should be noted that this study did not consider the effects of SiO_2 NPs on signaling pathways.

Additional studies are needed to better understand the contribution of signaling pathways to SiO_2 NP-induced retinal toxicity.

Declarations

Ethical Statement

All animal procedures were carried out in accordance with the National Institutes of Health Guide for the Care and Use of Laboratory Animals and were in compliance with the ARVO Statement for the Use of Animals in Ophthalmic and Vision Research. Animal protocols were approved by the Committee of Yantai University for the Care and Use of Laboratory Animals. All the procedures in this study were approved.

Author contributions

Zhuhong Zhang: Supervision and Writing. **Laien Zhao:** Investigation. **Yuanyuan Ma, Jia Liu** and **Yanmei Huang:** Methodology. **Xiaoxuan Fu, Shengjun Peng** and **Xiaojie Wang:** Data curation. **Yun Yang, Xiaoyan Zhang** and **Wanru Ding**Methodology and Data curation. **Jinguo Yu** and **Yanping Zhu:** Editing. **Hua Yan:** Supervision and Editing. **Shubin Yang:** Supervision and Methodology.

Conflict of Interest

The authors declare no conflict of interest.

Acknowledgments

This work was supported by funding from the National Natural Science Foundation of China (81970826 to Zhuhong Zhang and 22075241 to Shubin Yang) and the Talent Induction Program for Youth Innovation Teams in Colleges and University of Shandong Province (awarded to Yanping Zhu).

References

1. Liu X, Lu B, Fu J, Zhu X, Song E, Song Y. Amorphous silica nanoparticles induce inflammation via activation of NLRP3 inflammasome and HMGB1/TLR4/MYD88/NF-kb signaling pathway in HUVEC cells. J Hazard Mater. 2021;404:124050.
2. Vance ME, Kuiken T, Vejerano EP, McGinnis SP, Hochella MF Jr, Rejeski D, Hull MS. Nanotechnology in the real world: Redeveloping the nanomaterial consumer products inventory. Beilstein J Nanotechnol. 2015;6:1769–80.
3. Murugadoss S, Lison D, Godderis L, Van Den Brule S, Mast J, Brassinne F, Sebaihi N, Hoet PH. Toxicology of silica nanoparticles: an update. Arch Toxicol. 2017;91:2967–3010.
4. Sun JG, Jiang Q, Zhang XP, Shan K, Liu BH, Zhao C, Yan B. Mesoporous silica nanoparticles as a delivery system for improving antiangiogenic therapy. Int J Nanomedicine. 2019;14:1489–501.

5. Yang X, Liu J, He H, Zhou L, Gong C, Wang X, Yang L, Yuan J, Huang H, He L, et al. SiO2 nanoparticles induce cytotoxicity and protein expression alteration in HaCaT cells. Part Fibre Toxicol. 2010;7:1.
6. Wu X, Wu M, Zhao JX. Recent development of silica nanoparticles as delivery vectors for cancer imaging and therapy. Nanomedicine. 2014;10:297–312.
7. Hu C, Sun J, Zhang Y, Chen J, Lei Y, Sun X, Deng Y. Local Delivery and Sustained-Release of Nitric Oxide Donor Loaded in Mesoporous Silica Particles for Efficient Treatment of Primary Open-Angle Glaucoma. Adv Healthc Mater. 2018;7:e1801047.
8. Jo DH, Kim JH, Yu YS, Lee TG, Kim JH. Antiangiogenic effect of silicate nanoparticle on retinal neovascularization induced by vascular endothelial growth factor. Nanomedicine. 2012;8:784–91.
9. Panas A, Marquardt C, Nalcaci O, Bockhorn H, Baumann W, Paur HR, Mulhopt S, Diabate S, Weiss C. Screening of different metal oxide nanoparticles reveals selective toxicity and inflammatory potential of silica nanoparticles in lung epithelial cells and macrophages. Nanotoxicology. 2013;7:259–73.
10. Lee SY, Kim IY, Heo MB, Moon JH, Son JG, Lee TG. **Global Proteomics to Study Silica Nanoparticle-Induced Cytotoxicity and Its Mechanisms in HepG2 Cells**. *Biomolecules* 2021, 11.
11. Sergent JA, Paget V, Chevillard S. Toxicity and genotoxicity of nano-SiO2 on human epithelial intestinal HT-29 cell line. Ann Occup Hyg. 2012;56:622–30.
12. Brandao F, Costa C, Bessa MJ, Dumortier E, Debacq-Chainiaux F, Hubaux R, Salmon M, Laloy J, Stan MS, Hermenean A, et al: **Genotoxicity and Gene Expression in the Rat Lung Tissue following Instillation and Inhalation of Different Variants of Amorphous Silica Nanomaterials** (**aSiO2 NM**). *Nanomaterials (Basel)* 2021, **11**.
13. Abdel-Latif HMR, Shukry M, El Euony OI, Mohamed Soliman M, Noreldin AE, Ghetas HA, Dawood MAO, Khallaf MA. **Hazardous Effects of SiO2 Nanoparticles on Liver and Kidney Functions, Histopathology Characteristics, and Transcriptomic Responses in Nile Tilapia (Oreochromis niloticus) Juveniles**. *Biology (Basel)* 2021, 10.
14. Wang JJ, Sanderson BJ, Wang H. Cytotoxicity and genotoxicity of ultrafine crystalline SiO2 particulate in cultured human lymphoblastoid cells. Environ Mol Mutagen. 2007;48:151–7.
15. Chen X, Zhu S, Hu X, Sun D, Yang J, Yang C, Wu W, Li Y, Gu X, Li M, et al. Toxicity and mechanism of mesoporous silica nanoparticles in eyes. Nanoscale. 2020;12:13637–53.
16. Bourges JL, Gautier SE, Delie F, Bejjani RA, Jeanny JC, Gurny R, BenEzra D, Behar-Cohen FF. Ocular drug delivery targeting the retina and retinal pigment epithelium using polylactide nanoparticles. Invest Ophthalmol Vis Sci. 2003;44:3562–9.
17. Novack GD. Pharmacotherapy for the treatment of choroidal neovascularization due to age-related macular degeneration. Annu Rev Pharmacol Toxicol. 2008;48:61–78.
18. Penha FM, Rodrigues EB, Maia M, Furlani BA, Regatieri C, Melo GB, Magalhaes O Jr, Manzano R, Farah ME. Retinal and ocular toxicity in ocular application of drugs and chemicals–part II: retinal toxicity of current and new drugs. Ophthalmic Res. 2010;44:205–24.

19. Bhatnagar P, Spaide RF, Takahashi BS, Peragallo JH, Freund KB, Klancnik JM Jr, Cooney MJ, Slakter JS, Sorenson JA, Yannuzzi LA. Ranibizumab for treatment of choroidal neovascularization secondary to age-related macular degeneration. Retina. 2007;27:846–50.
20. Yu HJ, Ehlers JP, Sevgi DD, Hach J, O'Connell M, Reese JL, Srivastava SK, Wykoff CC. Real-Time Photographic- and Fluorescein Angiographic-Guided Management of Diabetic Retinopathy: Randomized PRIME Trial Outcomes. Am J Ophthalmol. 2021;226:126–36.
21. Tsang SH, Sharma T. Drug-Induced Retinal Toxicity. Adv Exp Med Biol. 2018;1085:227–32.
22. Quan JH, Gao FF, Ismail H, Yuk JM, Cha GH, Chu JQ, Lee YH. Silver Nanoparticle-Induced Apoptosis in ARPE-19 Cells Is Inhibited by Toxoplasma gondii Pre-Infection Through Suppression of NOX4-Dependent ROS Generation. Int J Nanomedicine. 2020;15:3695–716.
23. Wang L, Chen C, Guo L, Li Q, Ding H, Bi H, Guo D. Zinc oxide nanoparticles induce murine photoreceptor cell death via mitochondria-related signaling pathway. Artif Cells Nanomed Biotechnol. 2018;46:1102–13.
24. Zhu S, Gong L, Li Y, Xu H, Gu Z, Zhao Y. Safety Assessment of Nanomaterials to Eyes: An Important but Neglected Issue. Adv Sci (Weinh). 2019;6:1802289.
25. Leung CC, Yu IT, Chen W. **Silicosis** *Lancet*. 2012;379:2008–18.
26. Yoshida T, Yoshioka Y, Takahashi H, Misato K, Mori T, Hirai T, Nagano K, Abe Y, Mukai Y, Kamada H, et al. Intestinal absorption and biological effects of orally administered amorphous silica particles. Nanoscale Res Lett. 2014;9:532.
27. Tassinari R, Martinelli A, Valeri M, Maranghi F. **Amorphous silica nanoparticles induced spleen and liver toxicity after acute intravenous exposure in male and female rats**. *Toxicol Ind Health* 2021:7482337211010579.
28. Rafieepour A, Pourahmad Jaktaji MRA, Khodagholi J, Peirovi F, Mehrabi H, Mohammadian Y. Y: The Effect of Particle Size on the Cytotoxicity of Amorphous Silicon Dioxide: An in Vitro Toxicological Study. Asian Pac J Cancer Prev. 2021;22:325–32.
29. Kim IY, Joachim E, Choi H, Kim K. Toxicity of silica nanoparticles depends on size, dose, and cell type. Nanomedicine. 2015;11:1407–16.
30. Nabeshi H, Yoshikawa T, Matsuyama K, Nakazato Y, Tochigi S, Kondoh S, Hirai T, Akase T, Nagano K, Abe Y, et al. Amorphous nanosilica induce endocytosis-dependent ROS generation and DNA damage in human keratinocytes. Part Fibre Toxicol. 2011;8:1.
31. Passagne I, Morille M, Rousset M, Pujalte I, L'Azou B. Implication of oxidative stress in size-dependent toxicity of silica nanoparticles in kidney cells. Toxicology. 2012;299:112–24.
32. Zhang Z, Ren Z, Chen S, Guo X, Liu F, Guo L, Mei N. ROS generation and JNK activation contribute to 4-methoxy-TEMPO-induced cytotoxicity, autophagy, and DNA damage in HepG2 cells. Arch Toxicol. 2018;92:717–28.
33. Gunes S, He Z, van Acken D, Malone R, Cullen PJ, Curtin JF. Platinum nanoparticles inhibit intracellular ROS generation and protect against cold atmospheric plasma-induced cytotoxicity. Nanomedicine. 2021;36:102436.

34. Ma Y, Li P, Zhao L, Liu J, Yu J, Huang Y, Zhu Y, Li Z, Zhao R, Hua S, et al. Size-Dependent Cytotoxicity and Reactive Oxygen Species of Cerium Oxide Nanoparticles in Human Retinal Pigment Epithelia Cells. Int J Nanomedicine. 2021;16:5333–41.
35. Abbasi F, Samaei MR, Hashemi H, Savardashtaki A, Azhdarpoor A, Fallahi MJ, Jalili M, Billet S. The toxicity of SiO2 NPs on cell proliferation and cellular uptake of human lung fibroblastic cell line during the variation of calcination temperature and its modeling by artificial neural network. J Environ Health Sci Eng. 2021;19:985–95.
36. Tisi A, Passacantando M, Lozzi L, Riccitelli S, Bisti S, Maccarone R. Retinal long term neuroprotection by Cerium Oxide nanoparticles after an acute damage induced by high intensity light exposure. Exp Eye Res. 2019;182:30–8.
37. Wong LL, Pye QN, Chen L, Seal S, McGinnis JF. Defining the catalytic activity of nanoceria in the P23H-1 rat, a photoreceptor degeneration model. PLoS One. 2015;10:e0121977.
38. Paiva MRB, Andrade GF, Dourado LFN, Castro BFM, Fialho SL, Sousa EMB, Silva-Cunha A. Surface functionalized mesoporous silica nanoparticles for intravitreal application of tacrolimus. J Biomater Appl. 2021;35:1019–33.
39. Qu W, Meng B, Yu Y, Wang S. Folic acid-conjugated mesoporous silica nanoparticles for enhanced therapeutic efficacy of topotecan in retina cancers. Int J Nanomedicine. 2018;13:4379–89.
40. Park JH, Jeong H, Hong J, Chang M, Kim M, Chuck RS, Lee JK, Park CY. The Effect of Silica Nanoparticles on Human Corneal Epithelial Cells. Sci Rep. 2016;6:37762.
41. Wang C, Hou H, Nan K, Sailor MJ, Freeman WR, Cheng L. Intravitreal controlled release of dexamethasone from engineered microparticles of porous silicon dioxide. Exp Eye Res. 2014;129:74–82.
42. Sung MS, Heo H, Eom GH, Kim SY, Piao H, Guo Y, Park SW. **HDAC2 Regulates Glial Cell Activation in Ischemic Mouse Retina**. *Int J Mol Sci* 2019, 20.
43. Petrache Voicu SN, Dinu D, Sima C, Hermenean A, Ardelean A, Codrici E, Stan MS, Zarnescu O, Dinischiotu A. Silica Nanoparticles Induce Oxidative Stress and Autophagy but Not Apoptosis in the MRC-5 Cell Line. Int J Mol Sci. 2015;16:29398–416.
44. Park MV, Neigh AM, Vermeulen JP, de la Fonteyne LJ, Verharen HW, Briede JJ, van Loveren H, de Jong WH. The effect of particle size on the cytotoxicity, inflammation, developmental toxicity and genotoxicity of silver nanoparticles. Biomaterials. 2011;32:9810–7.
45. Chen M, von Mikecz A. Formation of nucleoplasmic protein aggregates impairs nuclear function in response to SiO2 nanoparticles. Exp Cell Res. 2005;305:51–62.
46. Mittal S, Pandey AK. Cerium oxide nanoparticles induced toxicity in human lung cells: role of ROS mediated DNA damage and apoptosis. Biomed Res Int. 2014;2014:891934.
47. Park EJ, Park K. Oxidative stress and pro-inflammatory responses induced by silica nanoparticles in vivo and in vitro. Toxicol Lett. 2009;184:18–25.
48. Moris D, Spartalis M, Tzatzaki E, Spartalis E, Karachaliou GS, Triantafyllis AS, Karaolanis GI, Tsilimigras DI, Theocharis S. The role of reactive oxygen species in myocardial redox signaling and

regulation. Ann Transl Med. 2017;5:324.

49. Ghiazza M, Polimeni M, Fenoglio I, Gazzano E, Ghigo D, Fubini B. Does vitreous silica contradict the toxicity of the crystalline silica paradigm? Chem Res Toxicol. 2010;23:620–9.

Scheme

Scheme 1 is available in supplementary section.

Figures

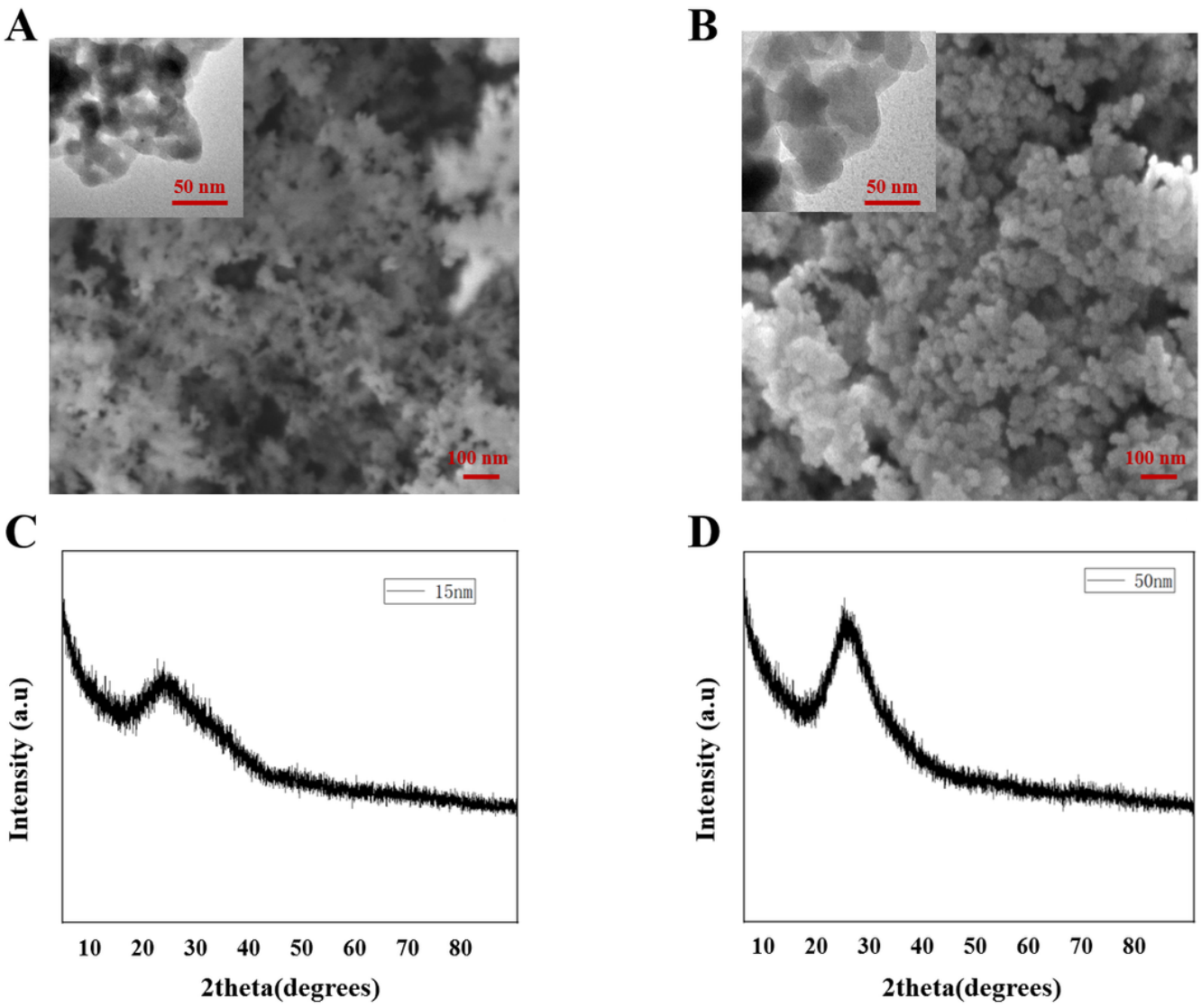

Figure 1

Characterization of SiO_2 NPs. SEM and TEM (insets) images of (A) 15-nm SiO_2 NPs and (B) 50-nm SiO_2 NPs. XRD spectra of 15-nm SiO_2 NPs (C) and 50-nm SiO_2 NPs (D).

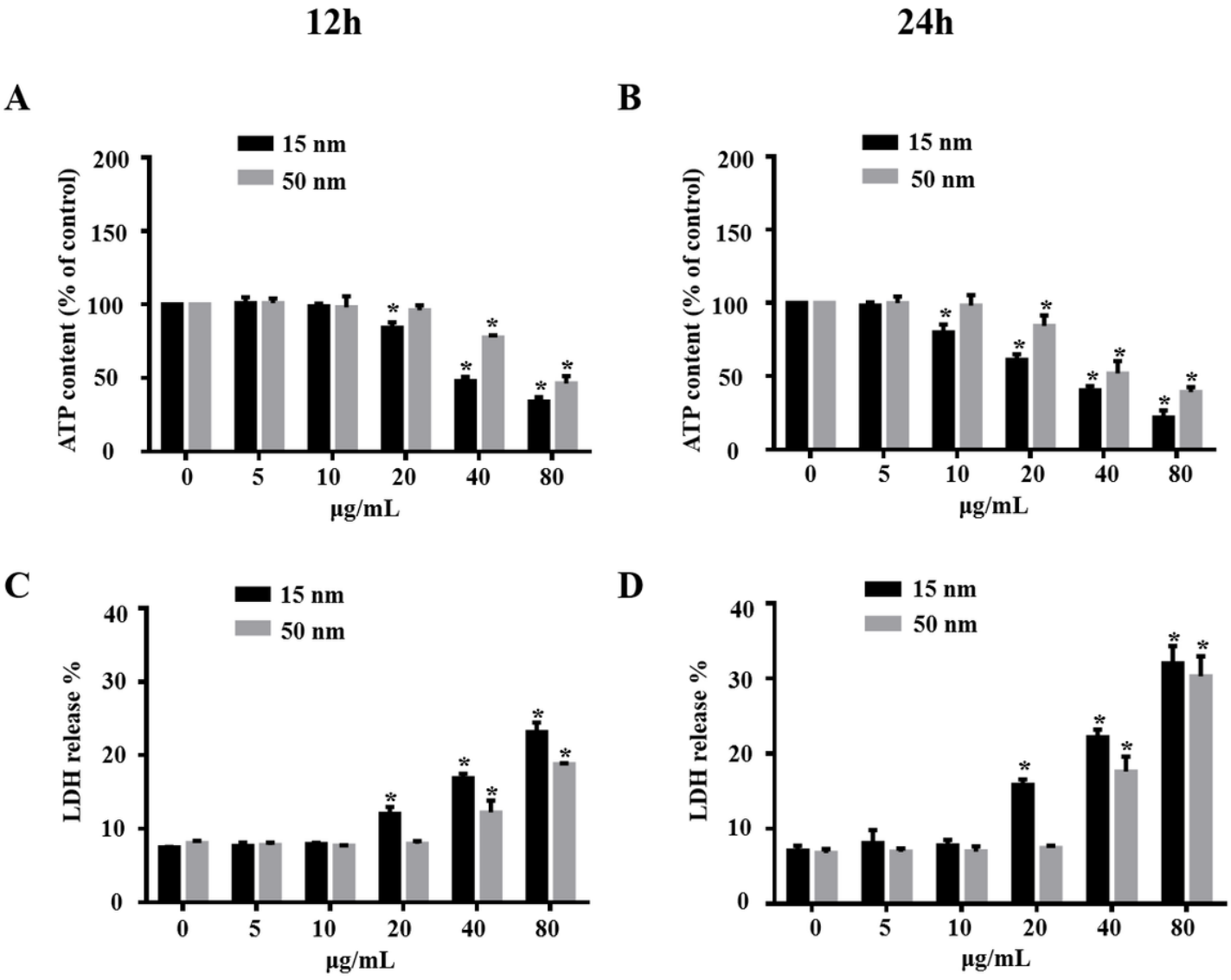

Figure 2

SiO_2 NPs induce cytotoxicity in R28 cells. R28 cells were exposed to different concentrations (5–80 μg/mL) of SiO_2 NPs for (A and C) 12 h and (B and D) 24 h before measurements of (A and B) ATP content and (C and D) LDH release. Data points represent the mean ± SD from three independent experiments with three samples per concentration in each experiment. *$p < 0.05$ compared to the control.

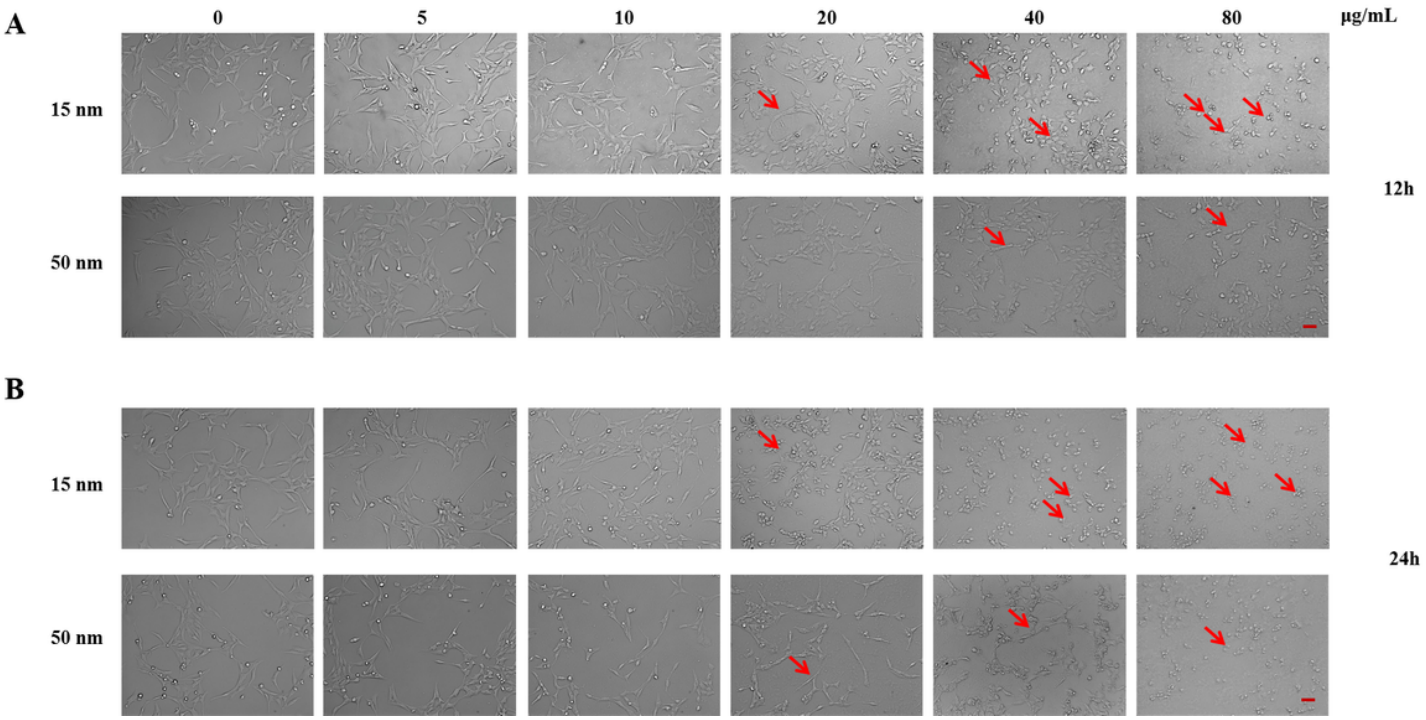

Figure 3

SiO_2 NPs induce morphological changes in cells. Morphological changes were observed via microscopy in R28 cells after 12 h (A) and 24 h (B) of exposure to 15- and 50-nm SiO_2 NPs at the indicated concentrations. Scale bar: 25 μm.

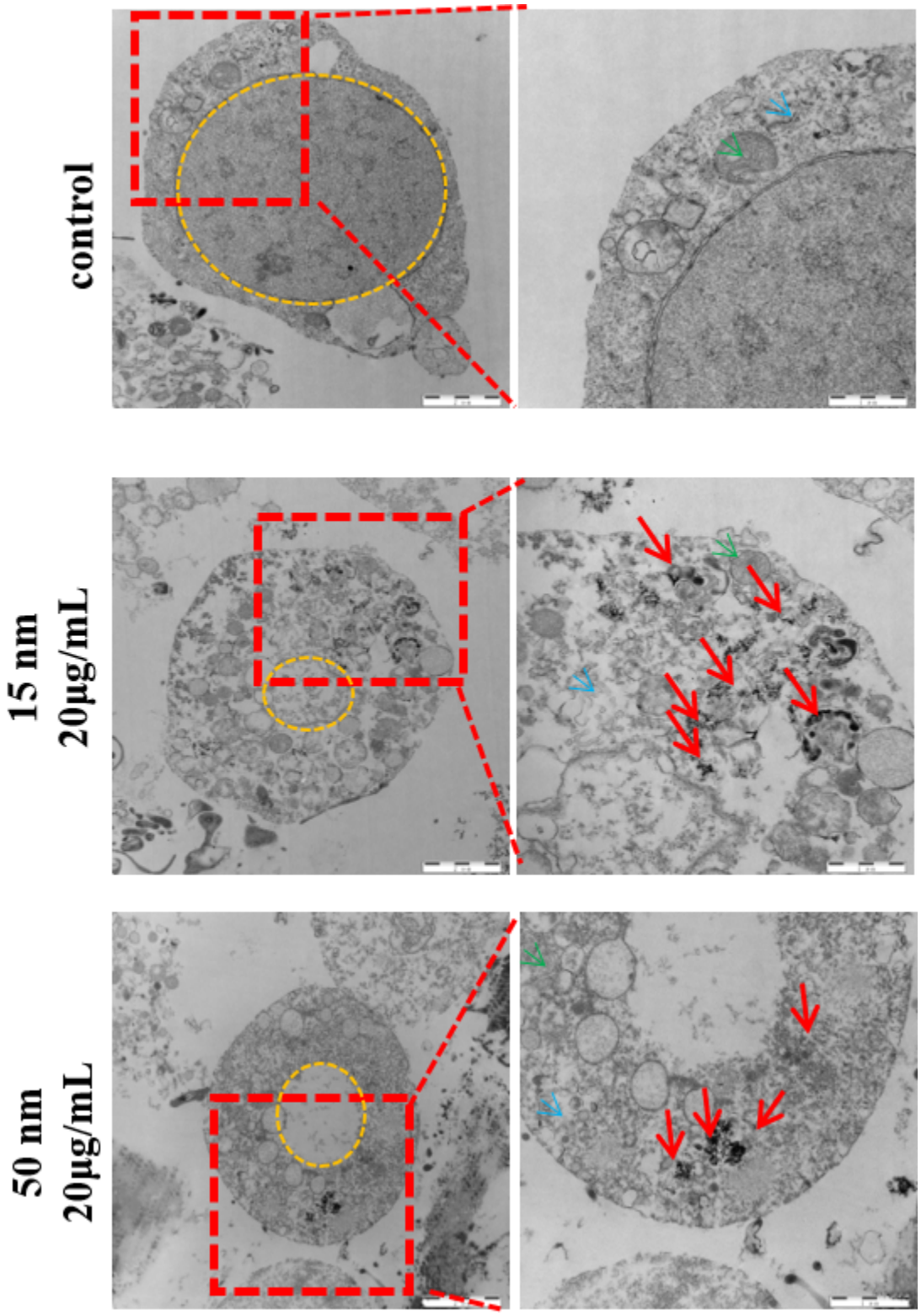

Figure 4

TEM evaluation of the cellular uptake and localization of 15- and 50-nm SiO_2 NPs in R28 cells over 12 h. Scale bars: 1 μm and 2 μm.

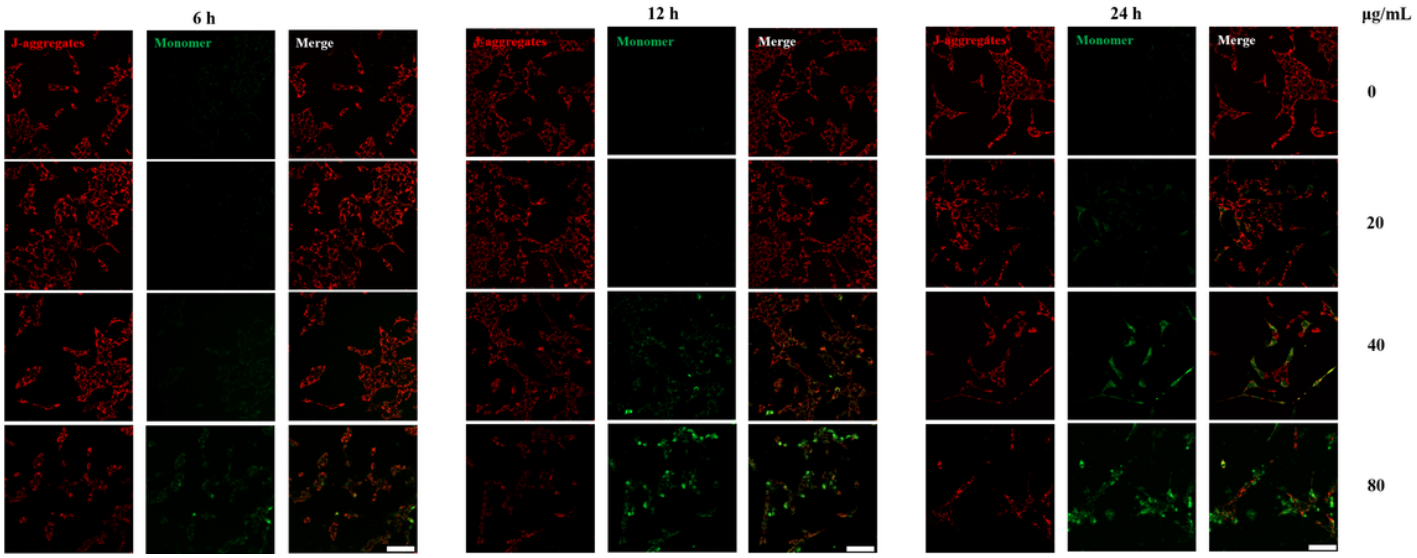

Figure 5

SiO_2 NPs induce mitochondrial dysfunction. R28 cells were treated with three concentrations (20, 40, and 80 μg/mL) of SiO_2 NPs for 6 h (A), 12 h (B) and 24 h (C), and mitochondrial membrane potential was evaluated by JC-1 staining. Scale bar: 50 μm.

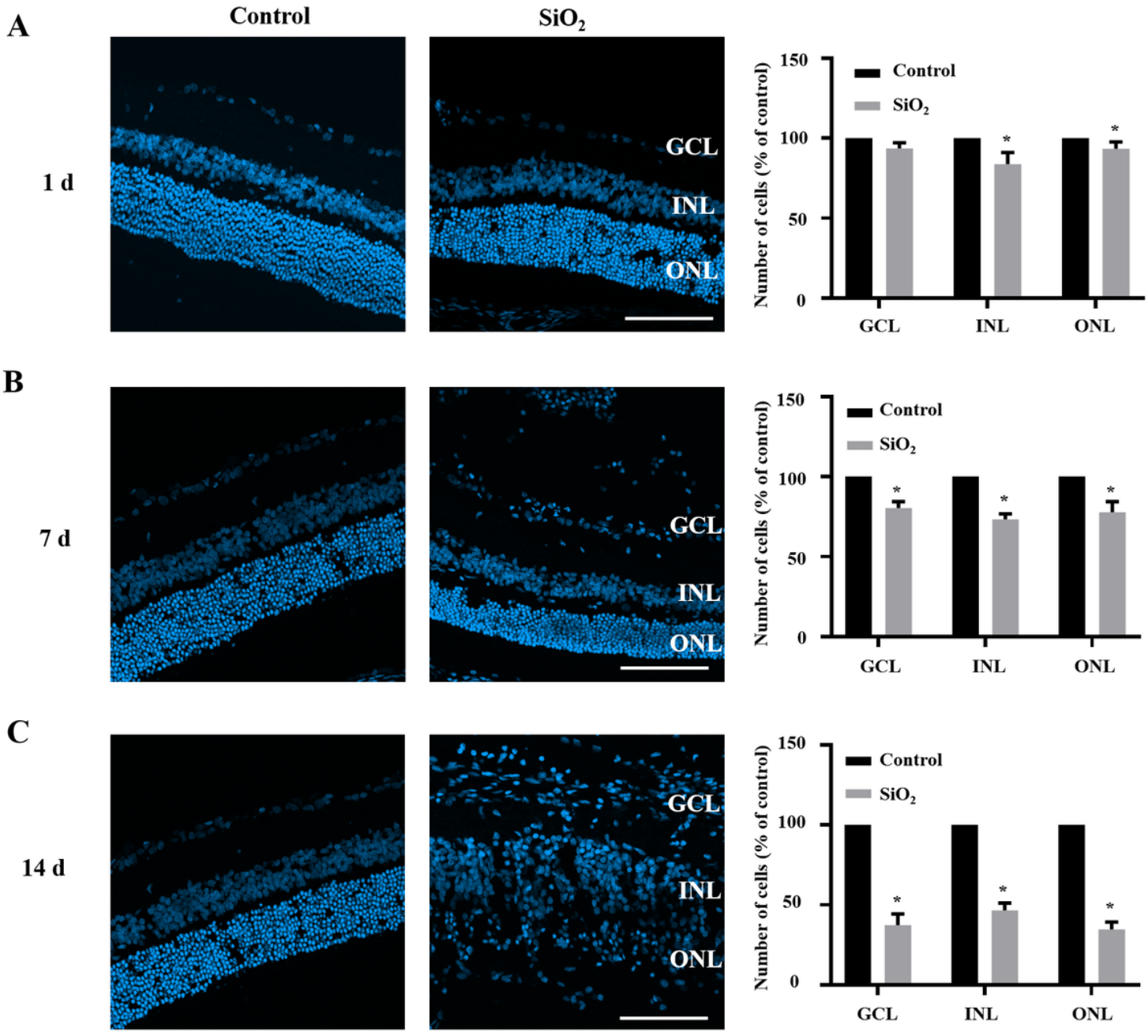

Figure 6

SiO_2 NPs decrease the number of retinal cells. PBS or 15-nm SiO_2 NPs were injected into the right eyes of rats. After euthanization, retinal sections were prepared for fluorescence microscopy. At 1 d (A), 7 d (B), and 14 d (C) after injection, the retinal layers (INL, GCL, and RGC layers) were stained by DAPI, and the cells in each layer were counted. Representative images are shown in the left panel, and the bar graph depicts the mean percentages of dead cells. *$p < 0.05$ compared to the vehicle control. Scale bar: 100 μm.

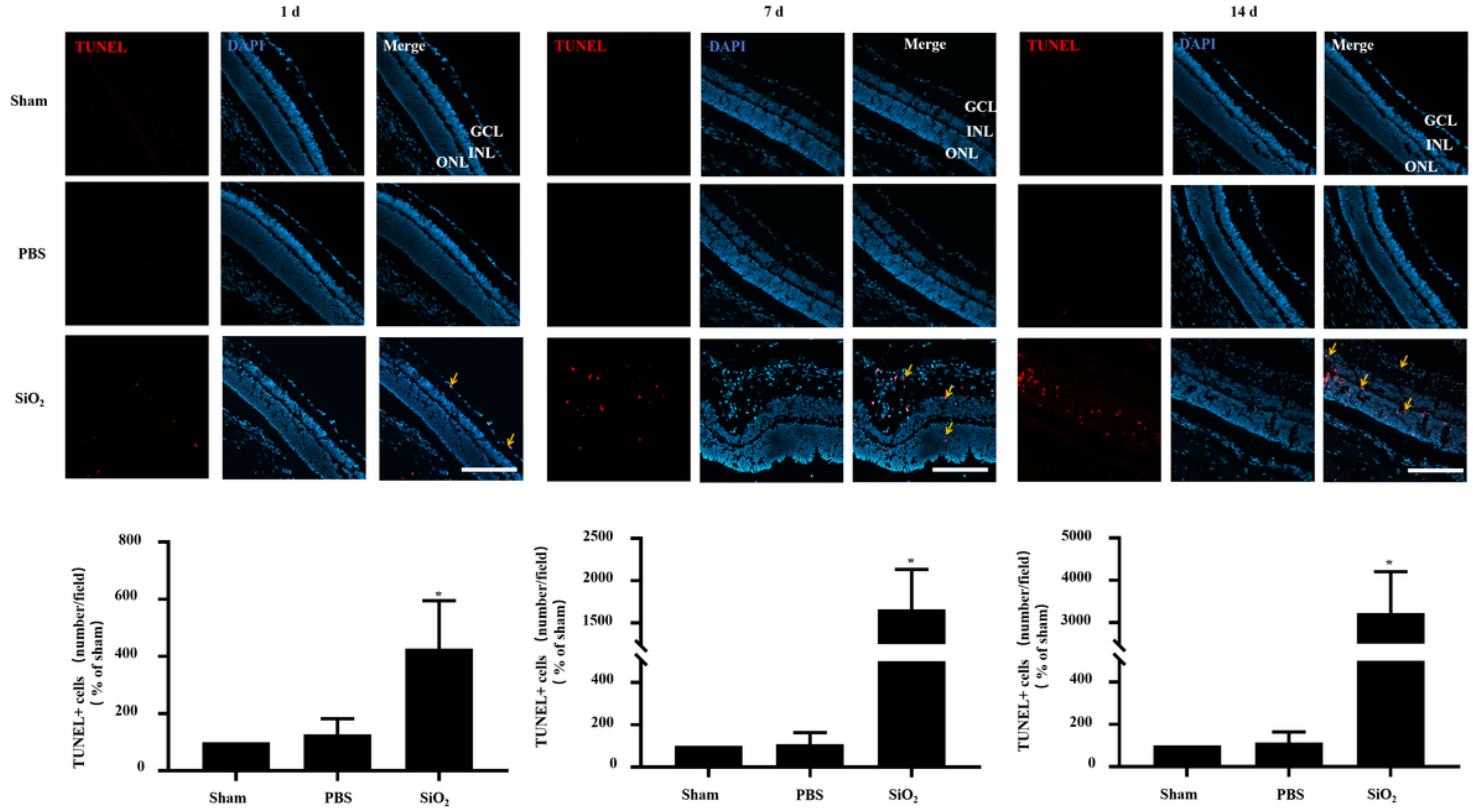

Figure 7

SiO_2 NPs cause apoptosis in rat retinas. Retinal sections were prepared as described in Fig. 6. At 1 d (A), 7 d (B), and 14 d (C) after SiO_2 NP injection, the retinas were analyzed by TUNEL assay (red = TUNEL; blue = DAPI). TUNEL-stained cells were observed in the GCL, INL, and ONL (orange arrows). Representative TUNEL staining images are shown in the upper panel. The bar graph depicts the mean percentages of apoptotic cells. *$p < 0.05$ compared to the sham group. Scale bar: 100 μm.

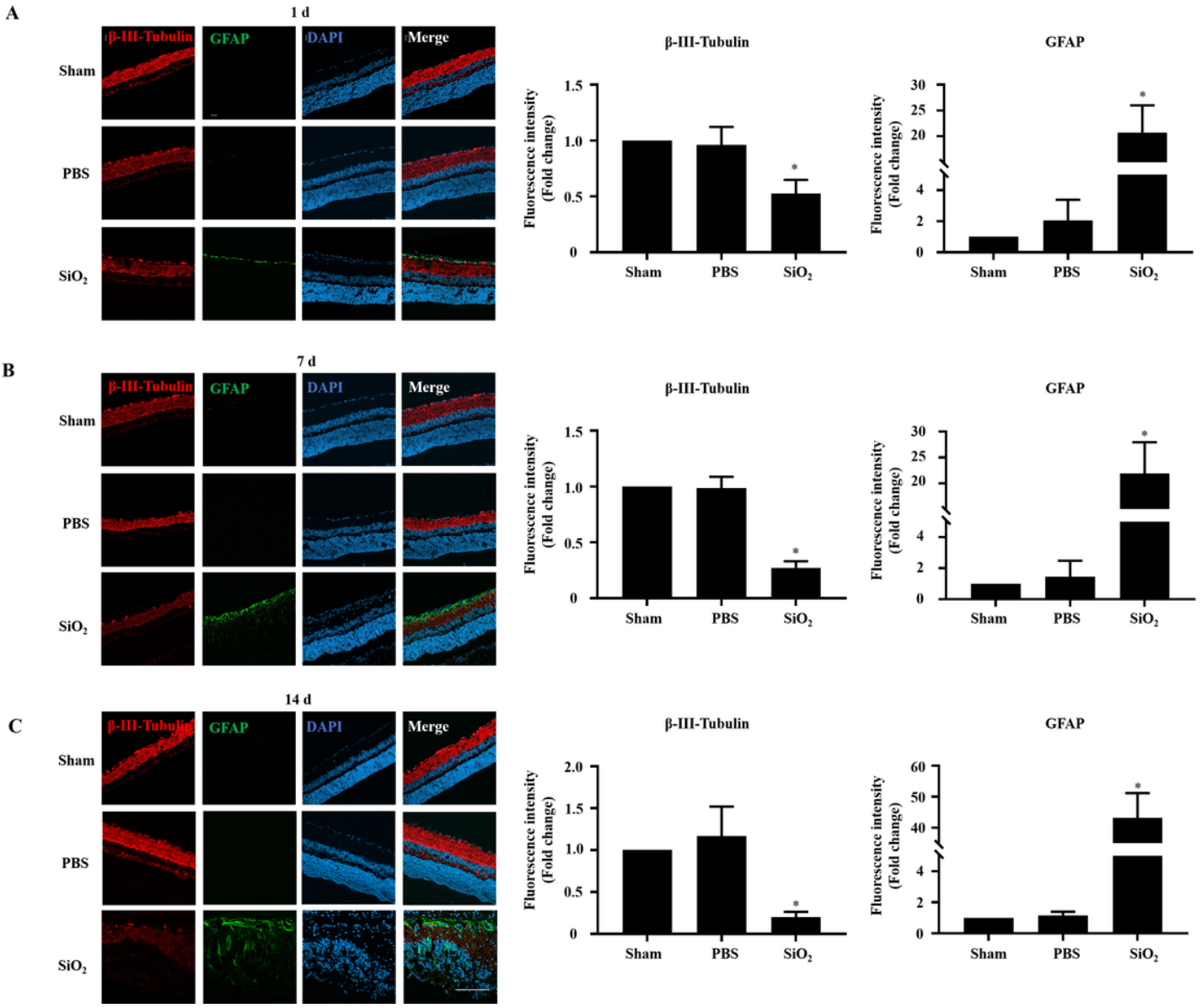

Figure 8

SiO_2 NPs induce the activation of retinal glial cells and reduce RGCs. Retinal sections were prepared as described in Fig. 6. At 1 d (A), 7 d (B), and 14 d (C) after SiO_2 NP injection, retinas were stained with the antibodies of β-III-tubulin (a marker of RGCs) and GFAP (a marker of glial cells). Representative images showing the distributions of β-III-tubulin (red) and GFAP (green). The bar graph depicts the mean fluorescence intensity. *$p < 0.05$ compared to the sham group. Scale bar: 100 μm.

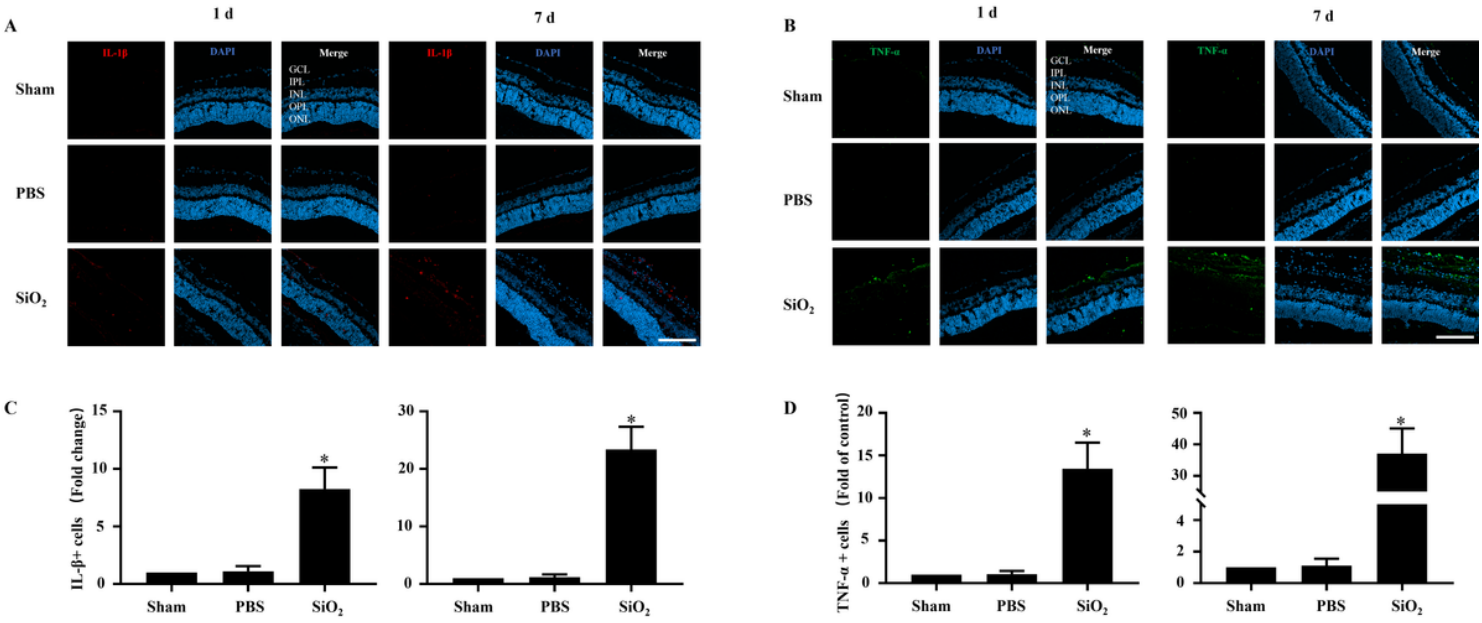

Figure 9

SiO_2 NPs cause the secretion of IL-1β and TNF-α. Retinal sections were prepared as described in Fig. 6. At 1 d (A and C) and 7 d (B and D) after SiO_2 NP injection, retinas were stained with the antibodies of TNF-α and IL-1β. Representative images showing the distributions of IL-1β (red) and TNF-α (green). The bar graph depicts the mean fluorescence intensity. *$p < 0.05$ compared to the sham group. Scale bar: 100 μm.

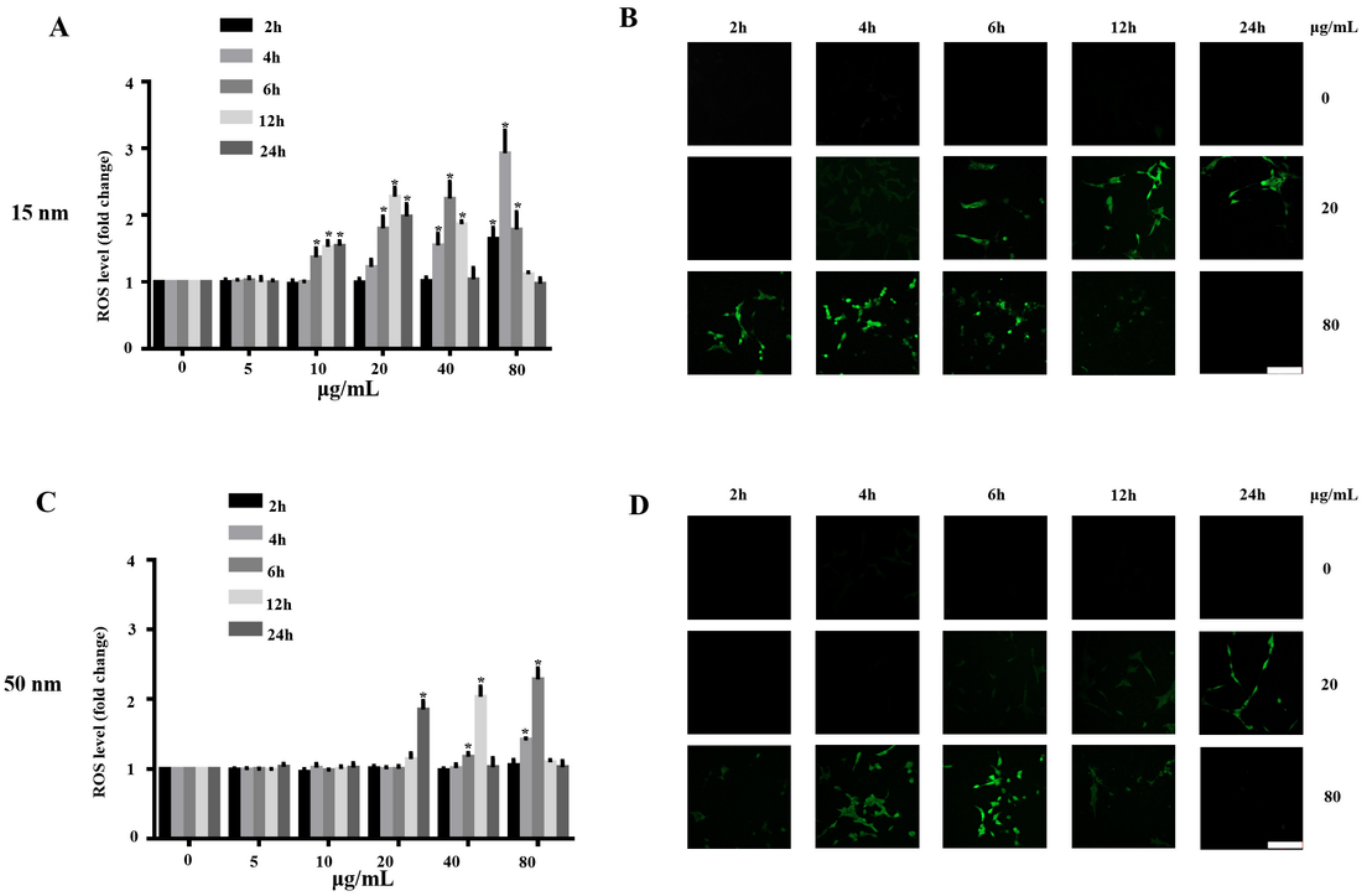

Figure 10

SiO_2 NPs induce ROS generation. ROS levels were measured by H_2DCF-DA staining at 2, 4, 6, 12 and 24 h after exposure to 15-nm (A) and 50-nm (C) SiO_2 NPs at various concentrations (5–80 μg/ml). (B and D) The ROS levels were monitored by CLSM, showing that ROS level increased with time after exposure to SiO_2 NPs at concentrations of 20 and 80 μg/mL. Data points are mean ± SD from three independent experiments with three samples per concentration. *$p < 0.05$ compared to the control. Scale bar: 100 μm.

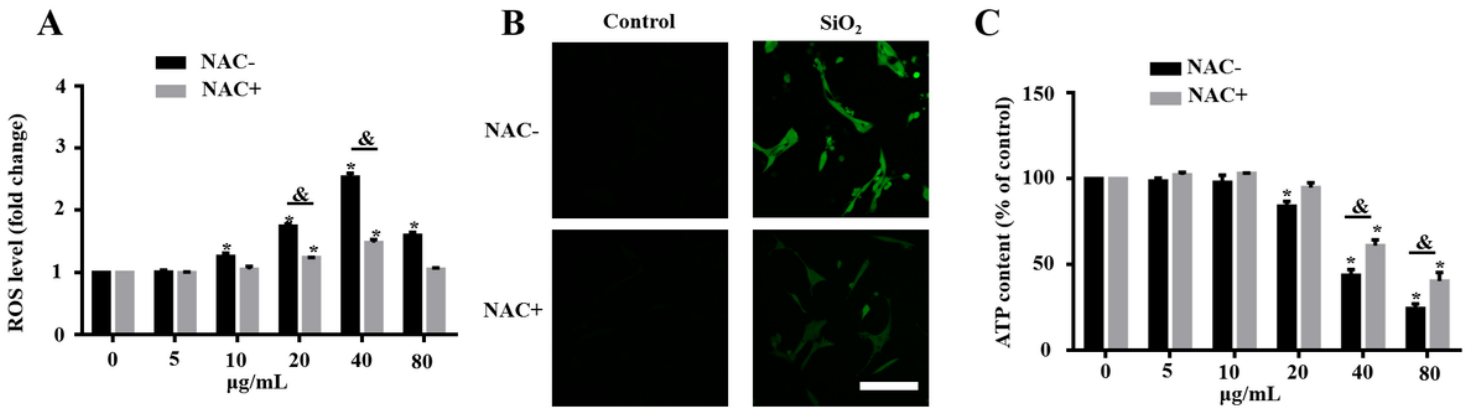

Figure 11

NAC attenuates SiO_2 NP-induced cytotoxicity. (A) Intracellular ROS levels were measured at 6 h after SiO_2 NP treatment with and without pretreatment with 10 mM NAC for 1 h. (B) ROS levels were monitored by CLSM, which showed that the ROS level increased at 6 h after exposure to SiO_2 NPs at a concentration of 40 μg/mL (C) ATP content was evaluated at 12 h after treatment with SiO_2 NPs with and without pretreatment with 10 mM NAC for 1 h. The data points are the mean ± SD from at least three independent experiments. *$p < 0.05$ compared to the vehicle control without NAC pretreatment; $^{\#}p < 0.05$ compared to the vehicle control with NAC pretreatment; $^{\&}p < 0.05$ between treatments with and without NAC pretreatment at the same concentration of SiO_2 NPs.

Supplementary Files

This is a list of supplementary files associated with this preprint. Click to download.

- Graphicalabstract2.docx
- Scheme01.png